Vortex–Vortex Interactions in the Winter Stratosphere

R. K. SCOTT

Northwest Research Associates, Bellevue, Washington

D. G. DRITSCHEL

School of Mathematics, University of St Andrews, Fife, Scotland

(Manuscript received 14 May 2005, in final form 1 July 2005)

ABSTRACT

This paper examines the interaction of oppositely signed vortices in the compressible (non-Boussinesq) quasigeostrophic system, with a view to understanding vortex interactions in the polar winter stratosphere. A series of simplifying approximations leads to a two-vortex system whose dynamical properties are determined principally by two parameters: the ratio of the circulation of the vortices and the vertical separation of their centroids. For each point in this two-dimensional parameter space a family of equilibrium solutions exists, further parameterized by the horizontal separation of the vortex centroids, which are stable for horizontal separations greater than a critical value. The stable equilibria are characterized by vortex deformations that generally involve stronger deformations of the larger and/or lower of the two vortices. For smaller horizontal separations, the equilibria are unstable and a strongly nonlinear, time-dependent interaction takes place, typically involving the shedding of material from the larger vortex while the smaller vortex remains coherent. Qualitatively, the interactions resemble previous observations of certain stratospheric sudden warmings that involved the interaction of a growing anticyclonic circulation with the cyclonic polar vortex.

1. Introduction

The stratospheric sudden warming is one of the most dramatic fluid dynamical phenomena in the terrestrial atmosphere. In the space of a few days the radiatively driven cyclonic circulation of the winter stratospheric polar vortex undergoes a rapid deceleration and polar temperatures increase abruptly. In extreme cases, so-called major warmings, the deceleration and temperature increase is such as to reverse the vertical shear and pole-to-equator temperature gradients throughout much of the stratosphere: zonal mean westerlies as strong as 80 m s^{-1} are replaced with easterlies and temperatures rise by several tens of degrees.

Traditionally, stratospheric sudden warmings are considered to result from the saturation and breaking of planetary waves, which propagate upward from a tropospheric source on the steep potential vorticity gradients around the polar vortex. This paradigm, based on a decomposition of the flow into wave and zonal mean components, was demonstrated in the pioneering mechanistic modeling work of Matsuno (1971) and Holton (1976) and has proved extremely useful, both in describing the dynamics of sudden warmings themselves and in quantifying the residual circulation responsible for long-term transport. In this view, major warmings typically fall into one of two categories, depending on whether the polar vortex is displaced off the pole (wave 1) or split (wave 2). Particularly dramatic examples of the latter include the warming of February 1979 (e.g., McIntyre and Palmer 1983) and the warming of September 2002 (e.g., Newman and Nash 2005), the only example of a Southern Hemispheric major warming on record. Recently, Esler and Scott (2005) showed that resonant excitation of a nonpropagating barotropic mode may provide the dominant forcing mechanism of these wave-2 sudden warmings.

Despite the success of the wave–mean flow description, the dynamics of the winter stratosphere often takes on a more local character. At these times, a description based on interactions of coherent structures of potential vorticity (PV) appears more natural than one

Corresponding author address: R. K. Scott, Northwest Research Associates, P.O. Box 3027, Bellevue, WA 98009-3027.
E-mail: scott@nwra.com

based on wave–mean flow interactions. This synoptic view was advocated by O'Neill and Pope (1988), who described the stratospheric evolution in terms of the interaction of vortices in the presence of topographic forcing in a numerical simulation of a sudden warming. A particularly striking example of vortex merger in the stratosphere was shown in Lahoz et al. (1996, their Fig. 16) during the Southern Hemisphere (SH) spring of 1994, when a traveling anticyclone merged with a quasi-stationary anticyclone in midlatitudes equatorward of the polar vortex edge. The interaction of the resulting anticyclone (also strengthening due to radiative effects) with the radiatively weakening polar vortex contributed to the ensuing final warming, when polar air was entrained into lower latitudes and the cyclonic circulation was replaced with anticyclonic circulation in the transition to summer easterlies.

Observations of the Northern Hemisphere winter stratospheric polar vortex reveal a persistent anticyclonic circulation and associated quasi-stationary ridge known as the Aleutian high located near 170°W on the equatorward side of the polar vortex edge (see, e.g., Harvey and Hitchman 1996, for a climatology). In the Southern Hemisphere, anticyclones are typically traveling during mid- and late winter, but may become quasi stationary in spring prior to the final warming (Lahoz et al. 1996). Using observations from the *Upper Atmosphere Research Satellite (UARS)* and the U.K. Met Office (UKMO) unified model, O'Neill et al. (1994) identified the merger of an eastward-traveling anticyclonic vortex with the Aleutian high prior to the sudden warming of January 1992. The interaction of the resulting anticyclonic circulation with the polar vortex contributed to the sudden warming a few days later. Various other studies (e.g., O'Neill and Pope 1988; O'Neill et al. 1994; Rosier and Lawrence 1999) have linked the evolution of the Aleutian high to the onset of stratospheric sudden warmings. Even when the polar vortex does not extensively break down, the interaction of the anticyclonic Aleutian high and the cyclonic polar vortex leads to entrainment of polar and midlatitude air and can contribute significantly to the mixing and transport of chemical species across the polar vortex edge (Lahoz et al. 1994, 1996).

The dynamics of interacting vortices in the winter stratosphere closely resembles the behavior of idealized vortex patches. Numerical studies of the vortex merger in the two-dimensional Euler equations date back to Christiansen and Zabusky (1973). More recently, Dritschel (1995) documented the equilibrium configurations of general two-dimensional vortices, including the case of oppositely signed vortices, and illustrated the nonlinear, time-dependent evolution of the unstable configurations using high-resolution contour dynamics. Of particular interest here is the result that, for two oppositely signed vortices of unequal sizes, the larger vortex generally exhibits the largest deformations, both at equilibrium and during instability. This result, which has also been observed for the case of three-dimensional Boussinesq vortices (Reinaud and Dritschel 2002; J. N. Reinaud and D. G. Dritschel 2004, unpublished manuscript), suggests the possibility that a relatively small Aleutian high may have a large effect on the dynamics of the polar vortex. Two further observations are in order: first, as vortex disturbances are large and the dynamics is far from linear, a wave–mean flow description is not a good representation of the evolution of vortex interactions; and, second, the time scales of vortex interactions in the stratosphere are much shorter than typical radiative time scales.

In this paper, we consider in detail the isolated interaction of two oppositely signed vortices in a compressible (i.e., non-Boussinesq) atmosphere. A main cyclonic vortex represents the polar vortex, while a generally smaller, anticyclonic vortex represents the Aleutian high, or the result of previous anticyclonic vortex merger. We use an adiabatic technique similar to that used by Dritschel (1995) to sweep out a family of stable equilibrium solutions, followed by high-resolution numerical integrations to follow the three-dimensional evolution of unstable configurations. Our results draw on earlier work (Scott and Dritschel 2005) that used the Green's function of the compressible system to show that a given PV anomaly has a stronger influence on the circulation above the level of the anomaly than below.

The structure of the paper is as follows. In section 2, we outline the experimental approach, physical parameters, and numerical procedures, and in particular the adiabatic technique for finding equilibria and constructing the initial conditions. In section 3, we describe properties of the equilibrium solutions including the orientation and deformation of the vortices at equilibrium and the dependence on circulation ratio and vertical offset. In section 4, we show examples of the time-dependent, nonlinear evolution of unstable equilibria and describe the results of a parameter sweep. In section 5, we consider the influence of the lower boundary. In section 6, we summarize our results and discuss their implications for stratospheric sudden warmings.

2. Approach

As a first approximation, we consider the polar vortex and Aleutian high as isolated (uniform) patches of anomalous cyclonic and anticyclonic potential vorticity, respectively. Although O'Neill and Pope (1988) identi-

fied an important role for tropospheric wave forcing in stratospheric vortex–vortex interactions, we restrict attention here to the unforced system to isolate as completely as possible the dynamics of the two-vortex system. Vortex–vortex interactions in the presence of topographic forcing will be considered in a future study.

The evolution of the system is completely governed by a relatively small set of parameters, including the size, shape, strength, and position of the vortices. We focus on varying two of these, namely, the relative circulation and vertical offset of the two vortices, while fixing the others to values representative of the winter stratosphere.

For each set of parameter values, equilibrium solutions are constructed using the adiabatic technique described in Dritschel (1995). Two spheroidal vortices, initially well separated, are pushed slowly together by an externally imposed, two-dimensional, area-preserving potential flow. The external flow is weak enough that the two vortices remain in approximate equilibrium as they become closer together, thus sweeping out a family of equilibrium solutions as a function of horizontal separation. The procedure is described in detail in section 2d below.

For small enough horizontal separation, the equilibria lose stability and a rapid interaction takes place. The nonlinear, time-dependent evolution of the vortex interactions is followed using the contour-advective semi-Lagrangian method developed by Dritschel and Ambaum (1997). The computational efficiency of this method allows a complete investigation of the two-dimensional parameter space described above, without compromising horizontal resolution.

a. Governing equations

For computational efficiency and for a succinct description of the large-scale, balanced dynamical motion, our model is based on the quasigeostrophic equations in a compressible (non-Boussinesq) atmosphere. This system is arguably the simplest geophysically relevant model of rotating, stratified flow. Since time scales for vortex–vortex interactions are short relative to the radiative time scale, we include no diabatic forcing term.

The governing equations are

$$\frac{Dq}{Dt} \equiv \frac{\partial q}{\partial t} + \mathbf{u} \cdot \nabla q = 0, \tag{1a}$$

$$\nabla_h^2 \psi + \frac{1}{\rho_0} \frac{\partial}{\partial z} \left(\rho_0 \frac{f^2}{N^2} \frac{\partial \psi}{\partial z} \right) = q, \tag{1b}$$

$$(u, v) = \left(-\frac{\partial \psi}{\partial y}, \frac{\partial \psi}{\partial x} \right), \tag{1c}$$

where $q(x, y, z, t)$ is the (anomalous) PV, ψ is the geostrophic streamfunction, $\mathbf{u} = (u, v)$ is the horizontal geostrophic velocity, ∇_h^2 is the horizontal Laplacian, x and y are horizontal coordinates, $z = -H \log p$ is an appropriate log pressure vertical coordinate, with vertical-scale height H, and $\rho_0 = \exp(-z/H)$ is the background density (cf. Pedlosky 1987). Here, $f = 2\Omega$ is the polar value of the Coriolis parameter, where $\Omega = 2\pi$ day^{-1} is the planetary rotation rate, and N is a constant buoyancy frequency.

b. Numerical details

We use the contour advective semi-Lagrangian algorithm developed originally by Dritschel and Ambaum (1997) and extended to cylindrical geometry by Macaskill et al. (2003). It solves (1) in a cylindrical domain using a polar coordinate system (r, θ, z) that rotates about the cylindrical axis $r = 0$ at the rate $\Omega = f/2$, where $f = 4\pi$ corresponds to the polar value of the planetary rotation rate. Lateral boundary conditions are free slip, and isothermal boundary conditions (i.e., $\psi_z = 0$) are imposed at the horizontal upper and lower boundaries at $z = 0$ and $z = Z_T$.

For the individual cases presented below, the equations are discretized using 64 layers in the vertical between $z = 0$ and $z = Z_T = 12\,H$, where the vertical-scale height $H = 6146$ m is representative of the stratosphere. Notionally, the vertical domain extends from the ground to near the top of the mesosphere. In the horizontal, the streamfunction and velocity fields are calculated on a stretched grid of 96 radial and 192 azimuthal points, although the PV itself is first interpolated onto a grid 4 times finer for more accurate inversion. The stretched grid concentrates radial grid points near the pole, distributing them uniformly in $r^{1/2}$ for improved resolution in the region of interest (providing about 30 radial grid points between the origin and a notional vortex edge at $r = 3L_R$, where $L_R = NH/f = 902$ km is the Rossby deformation radius). The lateral boundary is located at a distance of $R_{\text{out}} = 30\,L_R$ from the pole, far enough away to have practically no effect on the evolution.

For the parameter sweeps, a resolution of half the above was used, to permit a sufficiently dense sampling of the two-dimensional parameter space. The lower-resolution calculations gave results very similar to the corresponding high-resolution ones, particularly for the equilibrium states. During the time-dependent interactions, small differences between the low- and high-resolution cases developed, but these were restricted to the details of vortex filamentation; bulk features such as the wave activity and reduction in total circulation

TABLE 1. Fixed and varying parameters for the undisturbed polar vortex $\mathcal{V}_1$ and Aleutian anticyclone $\mathcal{V}_2$ in the two-vortex model: PV anomaly q; vertical–horizontal aspect ratio μ; vertical semiaxis c (in units of H); circulation ratio κ_2/κ_1; vertical offset $z_2 - z_1$, and polar vortex vertical centroid z_1 (both in units of H).

Fixed	$\mathcal{V}_1$	$\mathcal{V}_2$
q	1	-1
$\mu = c/a$	4/3	4/3
c	4	$4\lvert\kappa_2/\kappa_1\rvert^{1/3}$
Varying		
$-\kappa_2/\kappa_1$	0.02, 0.04, . . . , 0.98, 1	
$z_2 - z_1$	-2, -1.9, . . . , 1.9, 2	
z_1	6, 4.5	

were found to be largely insensitive to the resolutions considered.

c. Vortex parameters

As first approximations to the polar vortex and Aleutian high we consider spheroidal patches of uniform PV, labeled $\mathcal{V}_1$ and $\mathcal{V}_2$, respectively (subscripts 1 and 2 will also be used to identify physical quantities associated with $\mathcal{V}_1$ and $\mathcal{V}_2$). The two-vortex system can be described by the horizontal and vertical radii of each undisturbed vortex, their horizontal and vertical separations, and the ratio of the PV anomalies. For definiteness, we fix the vertical–horizontal aspect ratio of each vortex, $\mu = c/a$, to a value of $4H/3L_R$. This value is representative of the stratospheric polar vortex. Further, we fix the size of $\mathcal{V}_1$ to a representative stratospheric value, with a total depth of 8 H and horizontal radius of 3 L_R.

The relative strengths of the two vortices are determined by their volume and PV anomaly. It turns out that the nature of the interactions depends most significantly on the ratio of the product of these quantities, that is, on the ratio of the vortex circulations, defined by $\kappa_i = q_i V_i$, where $i = 1, 2$, q_i is the PV anomaly, and $V_i = 4\pi c_i a_i^2/3$ is the volume of the undisturbed vortex. This allows us to fix $q_1 = -q_2$ and vary the ratio κ_2/κ_1 through the size of $\mathcal{V}_2$, which is determined completely by c_2.

With this reduction, the system depends on the circulation ratio κ_2/κ_1, the vertical positions z_1 and z_2, and the horizontal separation $d = [(x_2 - x_1)^2 + (y_2 - y_1)^2]^{1/2}$, where (x_i, y_i, z_i) is the position of each vortex centroid in a Cartesian coordinate system. Of these, κ_2/κ_1, $z_2 - z_1$, and z_1 are treated as external parameters taking the values shown in Table 1 (which also summarizes the choices of fixed parameters). The horizontal separation is swept out during the equilibrium-finding procedure described in section 2d.

Only two values of z_1 are considered because interactions depend predominantly on the vertical offset $z_2 - z_1$. As shown below, the results show only small quantitative differences between $z_1 = 6H$ and $z_1 = 4.5H$. Further, in terms of the stratospheric polar vortex, these two values bracket the range of plausible separations between the lowermost vortex and the ground, with separations of $2H \approx 12$ km and $0.5H \approx 3$ km, respectively (since $c = 4H$). Essentially, for $z_1 = 6H$ the main dynamical evolution takes place far enough above the lower boundary for boundary effects to be unimportant. The second value of $z_1 = 4.5$ was chosen as this corresponds to the separation where lower boundary effects begin to affect the evolution (see Scott and Dritschel 2005, for further details).

d. Equilibria

The equilibrium-finding procedure described in Dritschel (1995) and Legras and Dritschel (1993) begins with two vortices already at (stable) equilibrium, makes a small change to their horizontal separation, and allows the pair to adjust to a new equilibrium state. Practically, this is achieved by imposing a weak, area-preserving, z-independent, external velocity field throughout the domain, which advects each vortex toward the origin. The vortices become more deformed as they drift closer together while remaining in quasi equilibrium.

When the vortices are well separated, an equilibrium solution is given to a good approximation by two corotating spheroids. We therefore consider two initially spheroidal vortices whose centroids lie, without loss of generality, on the line $y = 0$ in the corotating frame of reference, at the points $(\pm x_0, 0)$. We use a value of $x_0 = R_{\text{out}}/\sqrt{3}$ to approximately minimize the combined influence of the circulation due to the image (in the cylindrical boundary) of the vortex and the circulation due to the opposite vortex. As the vortices are brought together, the rotation rate of the reference frame is adjusted to follow the vortex corotation, thereby ensuring that the vortex centroids remain on the line $y = 0$ at all times.

In this frame of reference, a suitable external velocity field is a simple straining flow of the form

$$(u, v) = \epsilon(-x, y), \tag{2}$$

whose nondimensional magnitude $\varepsilon = 0.05$ has been chosen by experimentation to be small enough to allow the vortices to adjust to equilibrium as they approach each other. One benefit of the form (2) is that the external flow becomes progressively weaker as the vortices approach each other and become more significantly

deformed. A family of stable equilibrium solutions are thus swept out over a range of horizontal separations until the separation becomes small enough that the system loses stability.

e. Time-dependent interaction

We study the time-dependent evolution of the instability by solving the full equations (1) with initial conditions obtained from the above equilibrium-finding procedure at small horizontal separation. At present, we do not have a precise method for determining exactly when the equilibria become unstable. However, an inspection of a large number of cases suggests that the vortices are always unstable when their deformation becomes sufficiently large. It turns out that a suitable measure of vortex deformation is given by the second and third elliptical moments, $M_i^{(2)}$ and $M_i^{(3)}$, where

$$M_i^{(2)} = \frac{1}{M_i} \int_{\mathcal{V}_i} \rho_0(z)[x^2 + y^2 - r_e^2(z)]\, dx\, dy\, dz, \qquad (3a)$$

$$M_i^{(3)} = \frac{1}{M_i} \int_{\mathcal{V}_i} \rho_0(x) y^3\, dx\, dy\, dz, \qquad (3b)$$

and where $M_i = \int_{\mathcal{V}_i} \rho_0\, dx\, dy\, dz$ is the total mass of the vortex and $r_e(z)$ is the mean horizontal radius at each level. We assume a nondimensional scaling of x and y such that $R_{\text{out}} = 1$. Here, $M_i^{(2)}$ measures the horizontal ellipticity of the vortex and $M_i^{(3)}$ measures the departure from symmetry in the y axis, which typically takes the form of a crescent-shaped deformation of the larger vortex. In all the cases studied, the system is unstable when the combination

$$\mathcal{M} = \max[M_i^{(3)}, 0.05 M_i^{(2)}] \qquad (4)$$

exceeds a certain threshold, $\mathcal{M}_c$. For unequally sized vortices the deformation involves larger $M_i^{(3)}$ and smaller $M_i^{(2)}$. When the vortices are of similar size, however, the asymmetry in the y axis is small and the deformation involves mainly $M_i^{(2)}$.

We choose the threshold value $\mathcal{M}_c = 0.0001$, which has been empirically determined to ensure that the system is well within the margin of instability. For marginally unstable vortices the instability is relatively weak, with smaller growth rates and weaker interaction than occurs during the merger of like-signed vortices.

3. Equilibrium solutions

We begin by considering the equilibrium solutions of two equal volume, vertically aligned, oppositely signed vortices. Obviously this configuration is not intended to resemble the winter stratosphere. Rather, it is useful because it illustrates the type of vortex deformations that occur in the absence of the asymmetries introduced by differences in size and vertical position. Such a configuration might conceivably be approached in SH spring before the onset of the final warming, when radiative effects weaken the polar vortex and strengthen the Australian high, but the dipole will translate and is unlikely to remain stable over the pole for long.

As described in section 2d, a family of steady states is swept out as the originally spheroidal vortices are slowly brought together. As the vortex separation decreases, the vortices deform by flattening in the direction of their alignment, predominantly on the innermost faces (see Fig. 1). For the extreme case on the right, which is actually within the margin of instability, the faces are almost touching and the top view resembles the limiting case for two-dimensional vortices described in Dritschel (1995, his Fig. 6e).

In addition to the flattening, the vortices also develop a vertical tilt with lower vortex levels closer together and upper levels farther apart. The tilting appears consistent with the vertical dependence of the induced circulation of each vortex. The exponential variation of the background density profile introduces an anisotropy in the quasigeostrophic Green's function, with slower decay above than below the vortex, which means that the induced circulation of a uniform vortex patch is stronger above the vortex than below (see Scott and Dritschel 2005, e.g., their Fig. 2). Considering the vortex pair as a stack of two-dimensional dipoles translating in the positive y direction (i.e., toward the top of Fig. 1d), the dipole at upper levels will tend to translate faster than that at lower levels. This will cause the pair to tilt along the y axis, as observed in the figure. To reduce the y tilt, the vortices tilt away from each other (in x) with height, thereby increasing the horizontal separation and reducing the strength of the circulation each vortex feels from its pair.

We now consider how the symmetry of the above equilibria is broken, first, when the vortices are of unequal sizes, and second, when they are vertically offset. Equilibria for unequal vortices with zero vertical offset are shown in Fig. 2 for circulation ratios of $-\kappa_2/\kappa_1 = 0.8$, 0.6, 0.4, and 0.2. The corresponding equal volume case was shown in Fig. 1d. Note that the equilibria shown are for $\mathcal{M}$ just exceeding $\mathcal{M}_c$, and represent more or less the limit of the equilibrium-finding procedure: although these equilibria are unstable, the growth rate of the instability up to these horizontal separations is small enough that significant departures from equilibrium have not yet occurred. As for the equal volume case, the vortices again become flattened toward each other and tilted away from each other with height. Per-

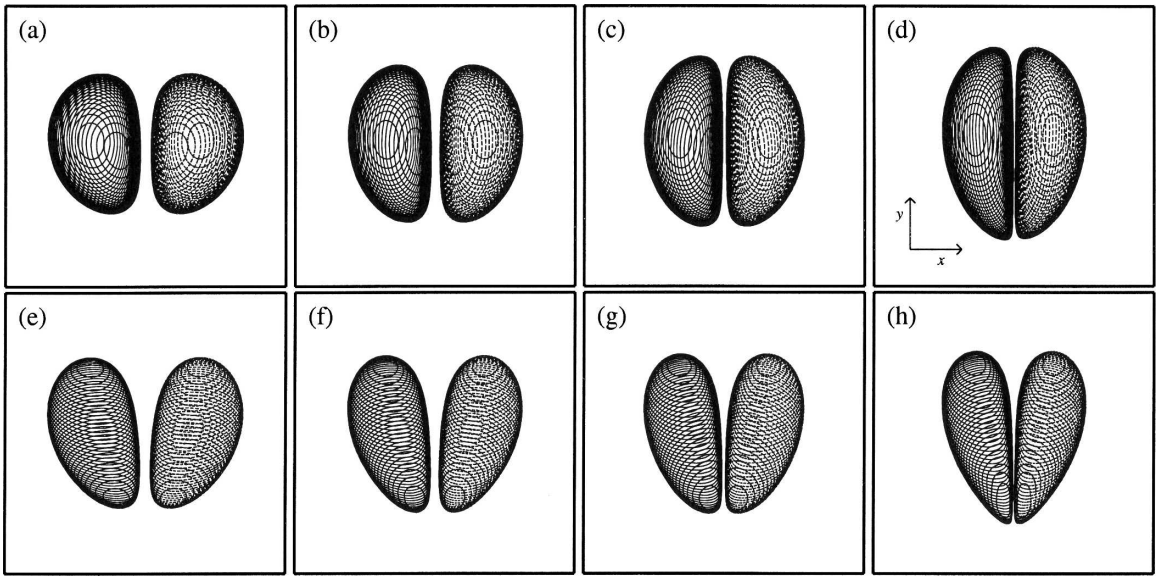

FIG. 1. Equilibrium states for the equal volume, vertically aligned vortex pair for different horizontal separations: (a)–(d) a top view and (e)–(h) side view perspective from an elevation of 30°. The negative (anticyclonic) vortex is drawn using dashed contours. The axis in (d) indicates the orientation relative to the Cartesian coordinates used in section 2c.

haps counterintuitively, however, it is the larger vortex that experiences the greatest deformation (see Fig. 2). Such behavior was identified already by Dritschel (1995) in the two-dimensional case and has also been observed in the three-dimensional Boussinesq case (J. N. Reinaud and D. G. Dritschel 2004, unpublished manuscript). In addition to flattening, the larger vortex also develops a characteristic concave shape oriented toward the smaller vortex.

Figure 3 shows the equilibria for the case of equal volume but vertically offset vortices, again at the point where $\mathcal{M}$ just exceeds $\mathcal{M}_c$. As the vertical offset is in-

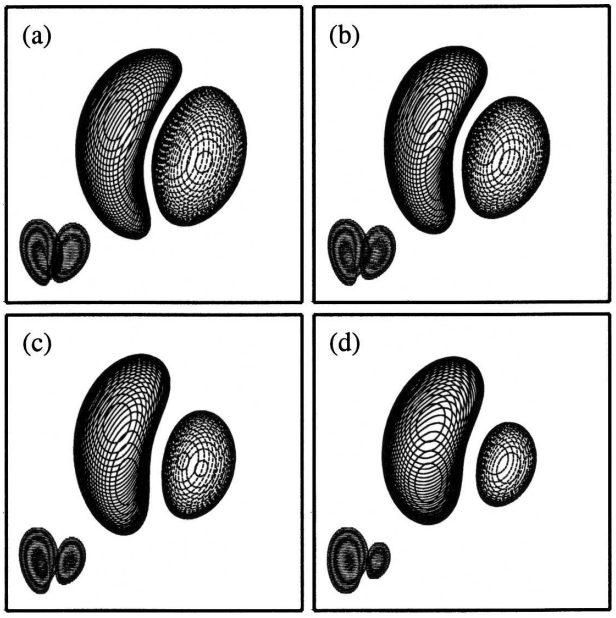

FIG. 2. Equilibrium states for vertically aligned vortex pairs of unequal volume: (a) circulation ratio $-\kappa_2/\kappa_1 = 0.8$, (b) $-\kappa_2/\kappa_1 = 0.6$, (c) $-\kappa_2/\kappa_1 = 0.4$, and (d) $-\kappa_2/\kappa_1 = 0.2$. The top view is shown large; the inset shows the corresponding side view.

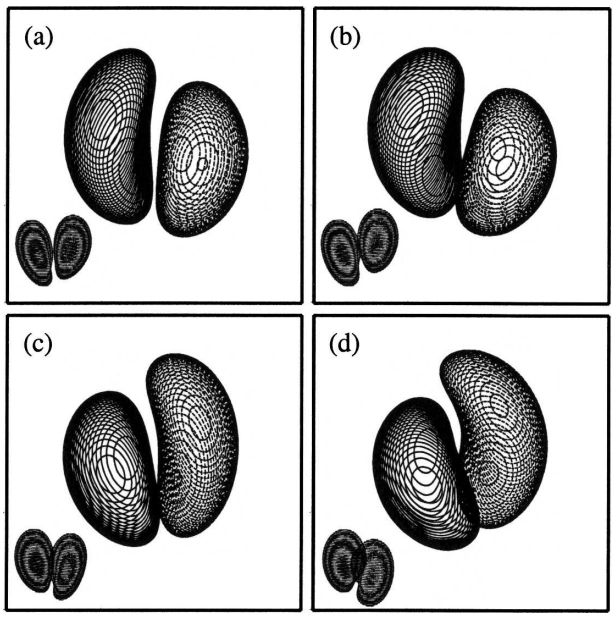

FIG. 3. Equilibrium states for equal volume vortex pairs with different vertical offsets: (a) $z_2 - z_1 = 0.8$, (b) $z_2 - z_1 = 1.6$, (c) $z_2 - z_1 = -0.8$, and (d) $z_2 - z_1 = -1.6$. The top view is shown large; the inset shows the corresponding side view.

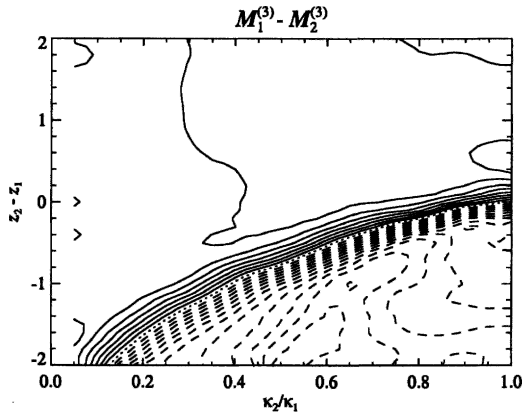

FIG. 4. Relative vortex deformation measured by the third moment, $M_i^{(3)} - M_2^{(3)}$, where $i = 1$ and 2 for the cyclonic and anticyclonic vortices, respectively. Positive values are contoured solid, negative values are dashed.

creased, the tilt of the vortices, which persists for small offsets, develops a twist, with the vortices partially wrapped together for $z_2 - z_1 = -1.6H$. We find that now the lower vortex is always the more deformed of the pair. As with the tilt, this property can be understood in terms of the slower decay of the Green's function above the vortex than below: at a given level, the circulation induced by the lower vortex is on average stronger than that induced by the upper vortex. The lower vortex can therefore be regarded in some sense as the stronger of the pair and experiences stronger deformation as in the case of unequal volume vortices. Note that the sense of the twist here is eastward with height, in contrast to the occasionally westward tilt with height of the Aleutian high (Harvey and Hitchman 1996), the latter is most likely a signature of upward wave propagation.

To quantify the combined effects of unequal volume and nonzero vertical offset on the vortex deformation we calculate, separately for each vortex, the third moment $M_i^{(3)}$, where $i = 1$ and 2 for the cyclonic and anticyclonic vortices, respectively. Figure 4 shows $M_1^{(3)} - M_2^{(3)}$ for circulation ratios $-\kappa_2/\kappa_1$ between 0.05 and 1 and vertical offsets $z_2 - z_1$ between $-2H$ and $2H$. As seen above, along the line $z_2 - z_1 = 0$ it is always the strongest vortex that is deformed the most. Similarly along the line $-\kappa_2/\kappa_1 = 1$ it is always the lower vortex that is deformed the most. In general, there is a well-defined crossover point in parameter space where the effects of vortex strength and vertical offset are in exact balance and the vortices are equally deformed. Above and to the left of that line (i.e., for a smaller and higher anticyclone) the cyclonic vortex experiences the most deformation.

4. Nonlinear evolution

We next consider the time-dependent evolution of unstable equilibrium solutions. As described in section 2e, we use the criterion $\mathcal{M} \geq \mathcal{M}_c$ to select unstable initial conditions from which to integrate the equations (1). For all the cases considered, this criterion ensures that the equilibria are indeed unstable. Although equilibria are often unstable at smaller values of $\mathcal{M}$ (i.e., at larger horizontal separation) the growth rate for the instability only becomes significant (relative to radiative relaxation rates in the stratosphere) at larger $\mathcal{M}$.

Figure 5 shows an example of the evolution of the instability for a circulation ratio $-\kappa_2/\kappa_1 = 0.6$ and vertical offset $z_2 - z_1 = 0$. The initial condition in Fig. 5a is the same as the equilibrium solution shown in Fig. 2b. As the instability develops, the cyclonic (polar) vortex becomes increasingly deformed, wrapping around the smaller, anticyclonic vortex. By $t = 6$ days the polar vortex has become so elongated that it wraps up into two distinct vortices, the smaller of these forming a dipole pair with the anticyclone. In addition to the shedding of a second vortex, the polar vortex also becomes highly tilted, which results in the subsequent shedding of vortex material at upper levels (not shown). Remarkably, the anticyclonic vortex remains coherent and approximately ellipsoidal throughout the evolution.

a. Parameter sweep

We use two measures to quantify the total deformation of the polar vortex resulting from the unstable interaction; namely, the time-averaged wave activity and the reduction in the zonal mean zonal velocity. The total wave activity $A(t)$ is the vertical integral of

$$A(z, t) = \rho(z) q \oint_{\Gamma(z)} [Y(\theta, z, t) - Y_e(z)]^2 \, d\theta, \qquad (5)$$

which represents the departure of the polar vortex from a circular cross section (Dritschel and Saravanan 1994). Here the integral is taken around a closed contour Γ (or collection of contours, if the original contour breaks up) at height z, θ is an azimuthal coordinate, $Y = \frac{1}{2} r^2$ (so that $dY\, d\theta$ is the differential area), $Y_e = \frac{1}{2} r_e^2$, and r_e is the radius of the undisturbed circular contour enclosing the same area as Γ. The total wave activity is normalized by the total angular impulse of the polar vortex at $t = 0$. Note that here we consider the wave activity of the polar vortex alone, as a measure of its deformation; the combined wave activity of the polar vortex plus anticyclone is conserved in the absence of dissipation.

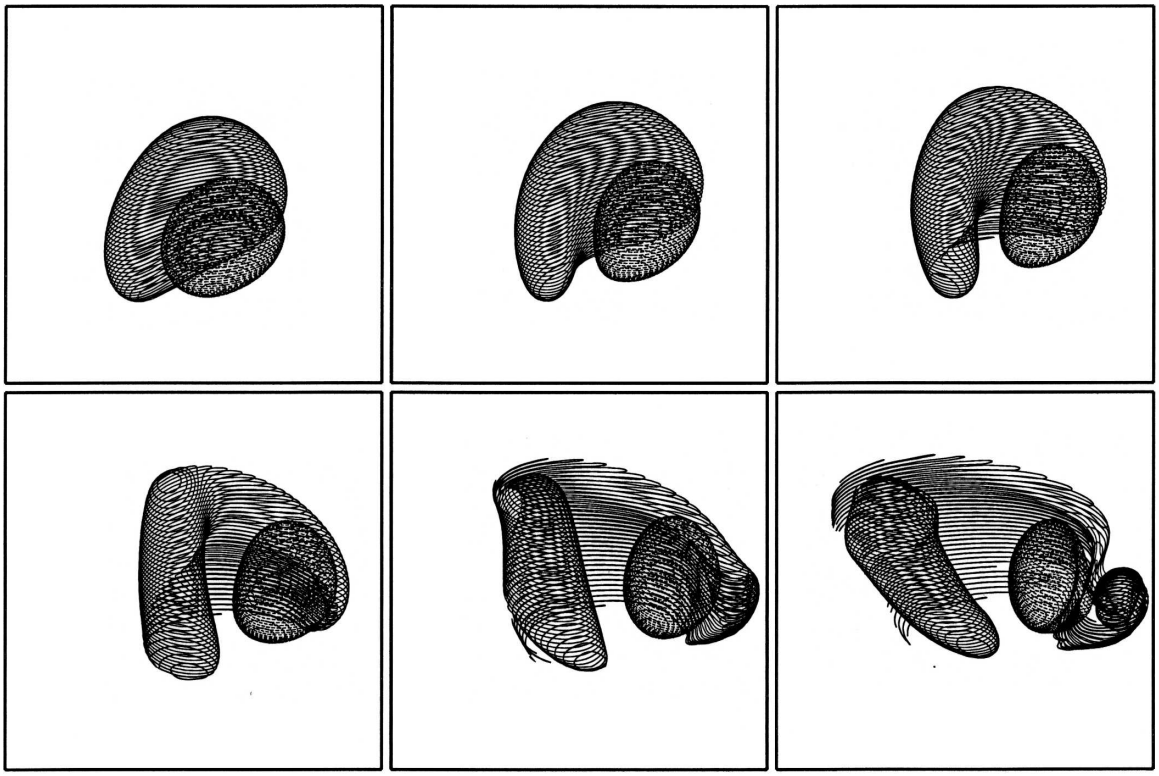

FIG. 5. Evolution for $-\kappa_2/\kappa_1 = 0.6$, $z_2 - z_1 = 0$ at $t = 0$, 2, 4, 6, 8, and 10 days (from upper left to lower right).

The reduction in zonal mean zonal velocity is defined as $[U(0) - U(\infty)]/U(0)$, where $U(t) = \max_{(r,z)}\overline{u}(r, z, t)$ is the domain maximum of the zonal mean zonal velocity at time t. The long-time value $U(\infty)$ is defined as the time average from $t = 10$ to $t = 40$. In calculating $\overline{u}$, we take the zonal mean to be the azimuthal average relative to the centroid of the polar vortex. While, at first sight, it is more natural to take the zonal mean relative to the global potential vorticity centroid, it is clear that such an approach fails for values of $-\kappa_2/\kappa_1$ nearing unity, when the global centroid is located increasingly distant from the region of interest. Our choice is motivated by our objective of quantifying the deformation of the polar vortex. Further, for small κ_2/κ_1 the difference between the polar vortex centroid and the global centroid is small. We note, however, that our choice differs from the traditional, geographically relative zonal mean used in spherical geometry in one important respect: on the sphere, the displacement of a vortex off the pole implies a deceleration of the traditional zonal mean zonal velocity, even in the absence of other vortex deformations. In contrast, taking the zonal mean relative to the vortex centroid implies that all zonal means are by definition translation invariant.

We calculate these two diagnostics for a series of simulations covering the two-dimensional parameter space defined by $-\kappa_2/\kappa_1$ and $z_2 - z_1$ taking the values shown in Table 1. Since the PV anomalies of each vortex are fixed, the range of circulation ratios corresponds to anticyclones of volumes between 1 and 1/20 times the volume of the polar vortex. The range of values of vertical offset allows for any vertical position of the anticyclone such that it remains entirely within the vertical domain. Negative offset values correspond to a lower anticyclone.

Figure 6 shows the results from the case $z_1 = 6H$, for which the polar vortex is in the center of the domain with the lowermost vortex level at a distance $2H$ from the ground. Both diagnostics show that significant interaction occurs over a highly localized region in parameter space. This region coincides closely with the transition region seen in Fig. 4 where both vortices have approximately equal levels of deformation. Thus, for $-\kappa_2/\kappa_1 < 1$, the maximum interaction, or the maximum effect of the anticyclone on the polar vortex, occurs for configurations in which the centroid of the anticyclone is slightly below that of the polar vortex. When the anticyclone is lower there is greater interaction with the lower, and denser, levels of the polar vortex, and hence there is a larger contribution to wave activity. On the other hand, if the anticyclone is too much lower it experiences stronger deformation than the polar vortex.

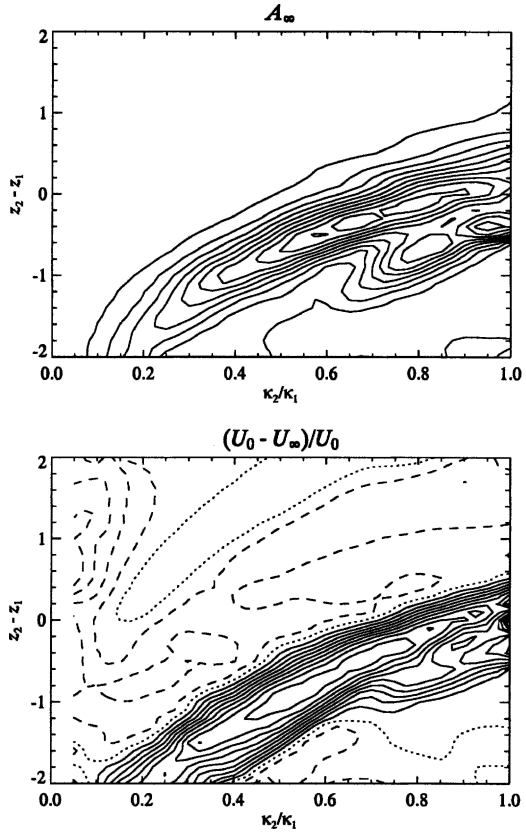

FIG. 6. Measures of the reduction in main (cyclonic) vortex intensity resulting from the interaction. (top) Total final wave activity of the cyclonic vortex normalized by the initial angular impulse. (bottom) Reduction in the domain maximum of the zonal mean zonal velocity $[U(0) - U(\infty)]/U(0)$. In both cases the subscript ∞ means the time average from $t = 10$ to $t = 40$ days. Zonal means are taken with respect to the centroid of the cyclonic vortex. Contouring is the same as in Fig. 4.

b. Dependence on vertical offset

We now examine in more detail the dependence of the vortex evolution on the vertical offset. Figure 7 shows the evolution at $t = 0, 4, 8$ days for $-\kappa_2/\kappa_1 = 0.6$ and values of vertical offset $z_2 - z_1 = 0.4H$, $-0.4H$, and $-0.8H$. See also the case $z_2 - z_1 = 0.0$ shown in Fig. 5. The maximum interaction occurs for $z_2 - z_1 = -0.4H$, consistent with Fig. 6a. Although a similar volume of material is shed from the polar vortex for $z_2 - z_1 = 0$, close inspection reveals that for $z_2 - z_1 = -0.4H$ material is shed from the vortex at lower levels and, because of density weighting, therefore results in a greater change in vortex angular momentum and wave activity. For $z_2 - z_1 = -0.8H$, material is shed from the polar vortex at still lower levels (the lowest contours being completely removed), although the volume is smaller. For $z_2 - z_1 = 0.4H$ (i.e., when the anticyclone is higher than the polar vortex), only a small volume of material is shed from the upper vortex levels and the density-weighted contribution to the angular momentum budget is small.

The distribution of zonal mean zonal velocity relative to the polar vortex centroid, $\overline{u}$, as a function of radial coordinate (corresponding to latitude) and height, also illustrates the relative strengths of interaction for different vertical offsets. Figure 8 shows $\overline{u}$ at (left column) $t = 0$ and (right column) $t = 10$ days for $z_2 - z_1 = 0.4$, 0, -0.4, -0.6, -0.8, and $-1.2H$, respectively. At $t = 0$ the polar vortex appears as a broad jet with a maximum between $r = 2\ L_R$ and $r = 3\ L_R$ and between $z = 7H$ and $z = 8H$, roughly corresponding to between 60° and 70° latitude and between 42- and 48-km height, not dissimilar to the winter stratospheric polar vortex. Depending on the height of the anticyclone, the interaction appears as a sudden deceleration of the jet with characteristics ranging from weak deceleration confined to the upper vortex ($z_2 - z_1 \geq -0.4H$) to complete reversal of $\overline{u}$ throughout most of the domain.

In terms of the deceleration of $\overline{u}$, the maximum effect of the anticyclone on the polar vortex is obtained for $z_2 - z_1 = -0.6H$ and $-0.8H$, where the zonal mean winds are reduced to around zero or reversed in a major sudden warming–like interaction. When the anticyclone is lower than this it has very little effect on the circulation of the polar vortex. When the anticyclone is higher its main effect is the reduction of zonal mean winds in the upper part of the domain only.

If we consider the appropriate scaling of vortex anomalies we find that time scales for the interaction are similar to those of stratospheric sudden warmings. With the chosen values of PV anomalies ($\pm f$), the maximum deceleration of the vortex is usually reached around $t = 10$ days. However, as can be seen from Fig. 8, these anomalies are somewhat weak, corresponding to a jet maximum of up to around 35 m s^{-1}, around half-typical stratospheric values. Doubling the PV anomalies to give more realistic zonal velocities is equivalent to halving the time scale: the same deceleration occurs as shown in Fig. 8 but with the contour interval of 10 m s^{-1} and over a time interval of 5 instead of 10 days, consistent with velocity changes and time scales of observed sudden warmings.

c. Dependence on circulation ratio

We now take a closer look at vortex interactions for different κ_2/κ_1. First, we consider the case of a very strong anticyclone, with $-\kappa_2/\kappa_1 = 0.8$. Although it is highly unlikely that a coherent anticyclone of this strength could ever develop in the winter stratosphere, it is not inconceivable that such a situation might arise in the Southern Hemisphere stratosphere in spring, im-

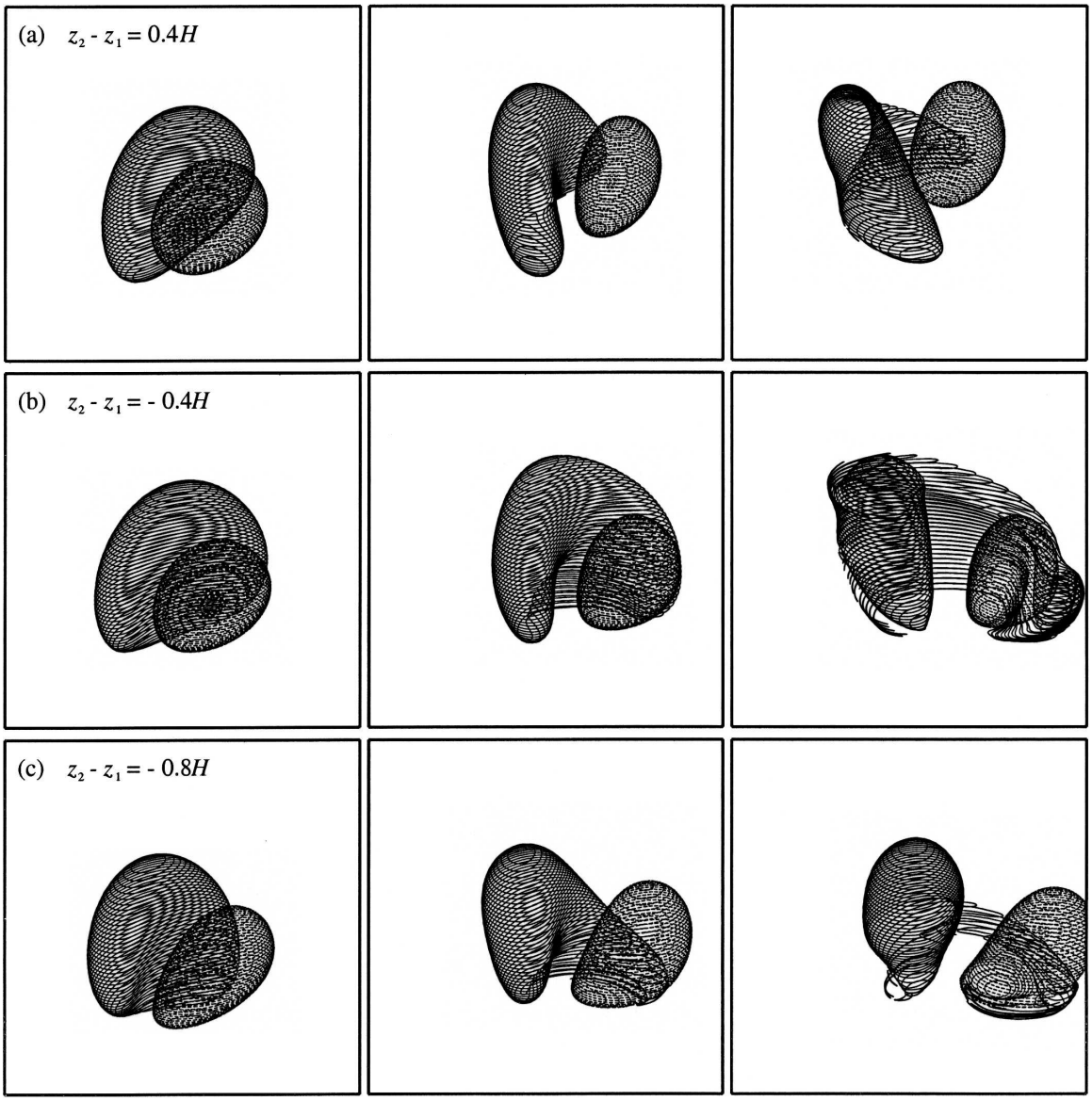

FIG. 7. Evolution for $-\kappa_2/\kappa_1 = 0.6$ at (left to right) $t = 0$, 4, 8 days: (a) $z_2 - z_1 = 0.4H$, (b) $z_2 - z_1 = -0.4H$, and (c) $z_2 - z_1 = -0.8H$.

mediately prior to the final warming, when radiative conditions are weakening the polar vortex and, in combination with dynamical processes, strengthening the Australian anticyclone. Figure 16 in Lahoz et al. (1996) indicates that anticyclonic circulations approaching the size of the polar vortex were present in the Southern Hemisphere middle stratosphere in October 1992.

The case of $-\kappa_2/\kappa_1 = 0.8$ and $z_2 - z_1 = 0$ is shown in Fig. 9 at times $t = 0$, 4, 8, 12, 16, and 20 days. At $t = 4$ the vortex begins to split in two approximately equal parts, these becoming increasingly separated by $t = 8$. Up until this time the anticyclone remains relatively coherent and undeformed. At $t = 8$, however, the anticyclone begins to interact with one of the separated remnants of the main vortex. Because of their semi-isolation from the other vortex remnant, their interaction follows the general pattern for two unequal vortices observed so far. Now, however, the anticyclone is the larger vortex, and the remnant the smaller, more coherent vortex, with the result that the anticyclone splits in two (from $t = 12$). The four vortices thus formed subsequently pair up and move apart under their induced circulation, apparently in a stable quasi equilibrium and with little further interaction.

The case of $-\kappa_2/\kappa_1 = 0.2$ is arguably more relevant to the winter stratospheric case. It illustrates that even a

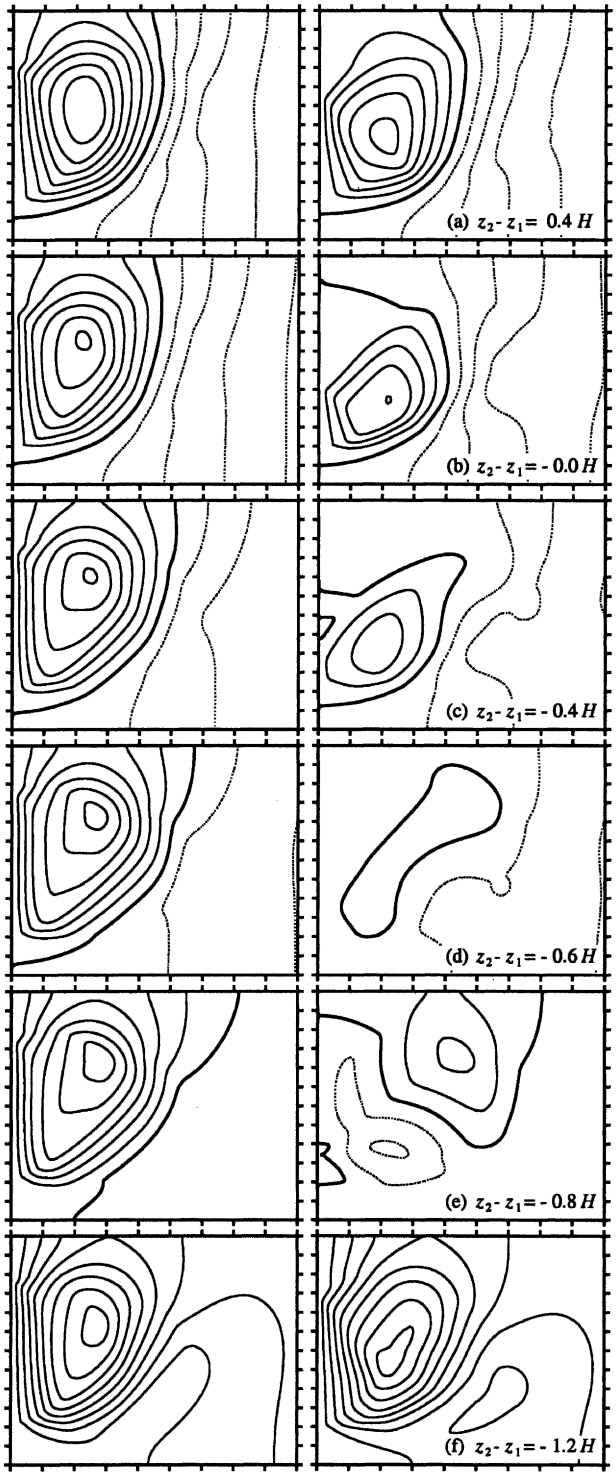

FIG. 8. Zonal mean zonal velocity, defined relative to the main (cyclonic) vortex centroid at (left) $t = 0$ and (right) $t = 10$ days, for the case $-\kappa_2/\kappa_1 = 0.6$ and for vertical offsets $z_1 - z_2 =$ (a) 0.4, (b) 0.0, (c) -0.4, (d) -0.6, (e) -0.8, and (f) $-1.2H$. Dotted contours denote negative values and the contour interval is 5 m s^{-1}.

relatively small anticyclone can induce a significant polar vortex deformation and deceleration of the vortex circulation if it lies at the appropriate vertical offset. Figures 10a,b show the cases $z_2 - z_1 = -1.2H$ and $z_2 - z_1 = -2.0H$, respectively, at times $t = 0$, 4, and 8 days. For $z_2 - z_1 = -1.2H$ material is pulled off the polar vortex from the central–lower levels. For $z_2 - z_1 = -2.0H$ less material is pulled off, but it consists of denser air from lower levels and has a potentially larger impact on the vortex angular momentum. Figures 11a,b show the corresponding zonal mean zonal velocity at $t = 0$ and $t = 10$, respectively. In each case the vortex is decelerated strongly, resembling a minor warming. The regions of strongest deceleration are different between the cases: deceleration is confined to the upper vortex for $z_2 - z_1 = -1.2H$, whereas it extends lower for $z_2 - z_1 = -2, 0H$. This pattern of deceleration is consistent with the stronger upward influence of PV anomalies in the compressible quasigeostrophic system identified previously by the authors (Scott and Dritschel 2005).

5. Lower boundary influence

The presence of a lower boundary has an important effect on the circulation induced by a PV anomaly in the compressible quasigeostrophic system. As shown in Scott and Dritschel (2005) the Green's function of a PV point anomaly close to a lower boundary contains a strong barotropic component with logarithmic horizontal dependence, which dominates the response away from the anomaly. In addition, the Green's function singularity at the lower boundary is doubled due to the image in the boundary, asymptoting to $-\frac{1}{2}\pi r$ for small r. For the dynamics of a single vortex, boundary effects were found to become important when the separation between the lowermost vortex and the lower boundary was around 0.5–1 density-scale heights.

Since in the above analysis, the polar vortex is situated at a separation of $2H$ from the lower boundary, it is important to establish whether the results hold at smaller separations. Boundary effects will potentially alter both the equilibrium solutions and the nonlinear interactions. We therefore repeated the analysis for $z_1 = 4.5H$, for which the lowermost level of the polar vortex is separated by only $0.5H$ from the lower boundary and boundary effects might be important. Although it is interesting to consider even smaller separations, these are less relevant to the stratospheric case, where the vortex is generally well separated from the ground. Our choice of $z_1 = 4.5H$ already corresponds to smaller separations than typically observed in the winter atmosphere.

It turns out that even at this small separation from

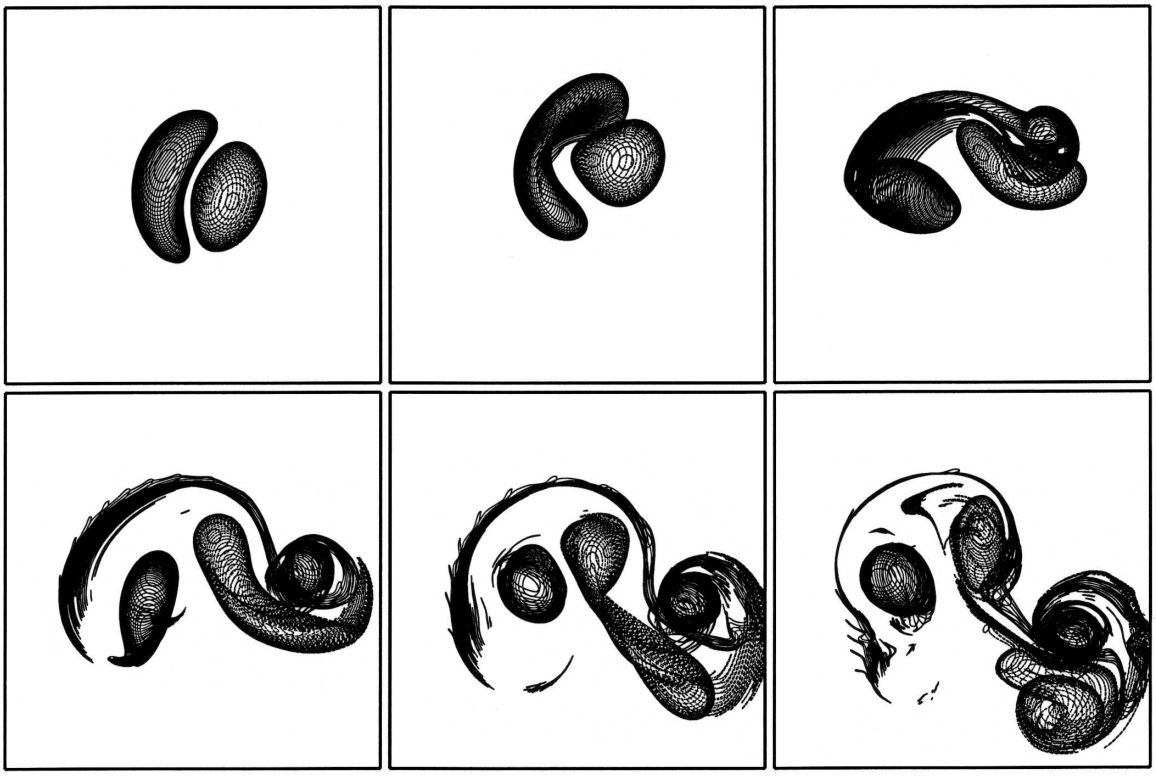

FIG. 9. Evolution for $-\kappa_2/\kappa_1 = 0.8$, $z_2 - z_1 = 0$, at $t = 0$, 4, 8, 12, 16, and 20 days (from upper left to lower right; top view).

the lower boundary, both equilibrium solutions and nonlinear interactions are qualitatively unchanged, although certain systematic differences are observed. For example, the equilibrium solutions such as those shown in Figs. 1–3 are in general characterized by a smaller vertical tilt, with the vortices in the lowermost levels less squashed together. This effect is likely due to the intensification of the Green's function singularity for PV close to the lower boundary. Similarly the lower levels of the vortices in general experience less deformation for $z_1 = 4.5H$ than for $z_1 = 6H$.

Because a greater fraction of the total vortex deformation occurs at upper levels for $z_1 = 4.5H$, the measure $\mathcal{M}$ will generally take smaller values than for $z_1 = 6H$, on account of the density weighting in (3). As a result, equilibria in the $z_1 = 4.5H$ case generally become unstable at lower values of $\mathcal{M}$, and it was found that a lower-threshold value of $\mathcal{M}_c = 0.00005$ was a more suitable indication of when to start the time-dependent evolution of the instability; higher values of $\mathcal{M}_c$ resulted in vortices that were clearly deformed well beyond their unstable equilibrium configuration.

Results of the time-dependent evolution of the instability are summarized in Fig. 12 for $z_1 = 4.5\ H$, corresponding to the parameter sweep discussed in section 4a and Fig. 6 above. Again, there is a well-defined region in parameter space over which the strength of the interaction is maximal. Note that, because of the constraint that both vortices lie entirely inside the domain, the parameter sweep is truncated at large negative vertical offset and circulation ratio; points on the boundary of the shaded region correspond to cases where the anticyclone exactly touches the lower boundary. Comparison of several individual cases (not shown) reveal some differences between the cases $z_1 = 4.5H$ and $z_1 = 6H$, for example, generally weaker tilting of the polar vortex and shedding of vortex material over a deeper vertical range for $z_1 = 4.5H$, presumably a result of the stronger barotropic component of the circulation. The main conclusions, however, are unchanged; namely, that the larger of the two vortices is always the more significantly deformed, that a relatively modest anticyclone can lead to substantial polar vortex deformations, and that the strongest interactions occur over roughly the same, well-defined region of parameter space.

6. Discussion

Although highly idealized, the above results were developed as a model of vortex interactions in the winter polar stratosphere. Our intention is to study processes of vortex interaction general enough that they do not

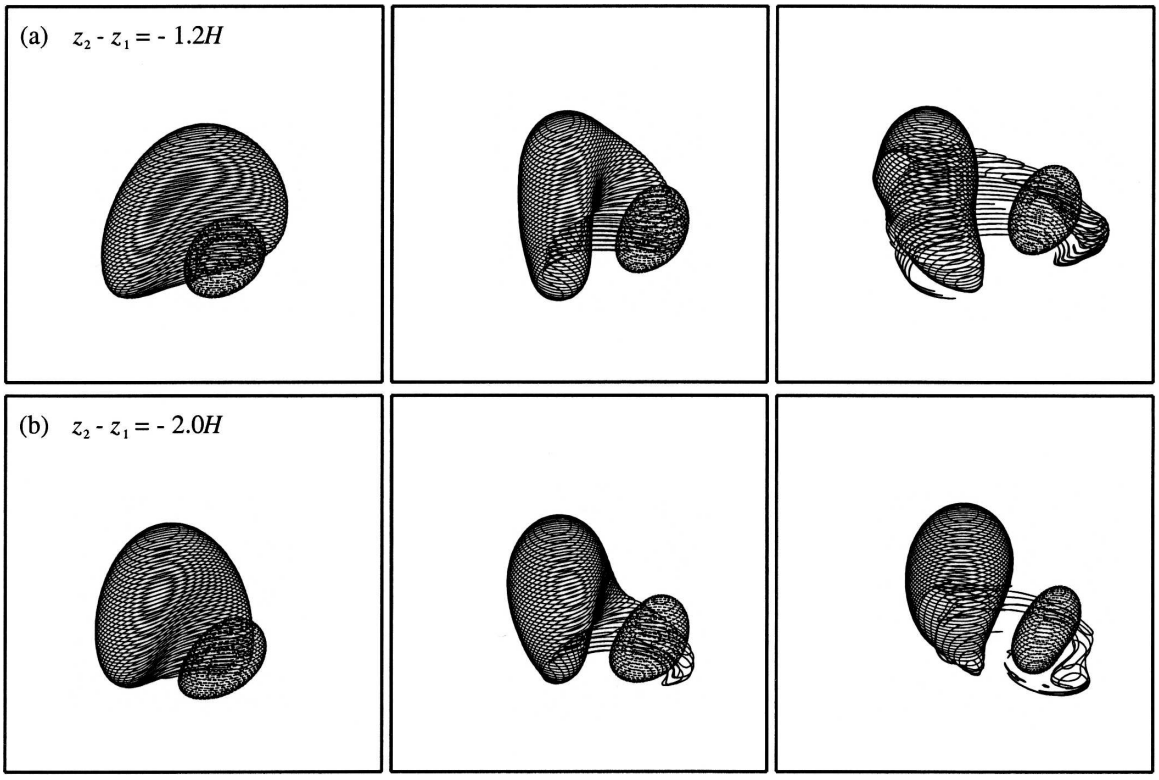

FIG. 10. Evolution for (a) $-\kappa_2/\kappa_1 = 0.2$, $z_2 - z_1 = -1.2H$ and (b) $z_2 - z_1 = -2.0H$ at $t = 0$, 4, and 8 days (left to right).

depend on the finer details of the model, but which are instead robust and fundamental properties of the fluid dynamical system. In our model, the larger, cyclonic vortex represents the polar vortex and the smaller, anticyclonic vortex represents the Aleutian high, or other similar anticyclonic circulations often observed in both the Northern and Southern Hemisphere winter stratospheres. The approximation of these structures by uniform, oppositely signed PV anomalies having a spheroidal undisturbed state leads to perhaps the simplest configuration possible in three dimensions, some might argue too simple. On the other hand, the zonal mean zonal velocity profile associated with these structures is not unrealistic (e.g., Fig. 8). Further, given the increasingly well-accepted view of the polar vortex edge as a region of intense PV gradients, the approximation of a vortex patch is in some respects better than, for example, the uniform PV gradient approximations used in pioneering work on wave propagation. We emphasize that our aim, in common with those early papers, is to investigate fundamental processes that might be relevant to the winter stratosphere, rather than to reproduce in detail the stratospheric evolution.

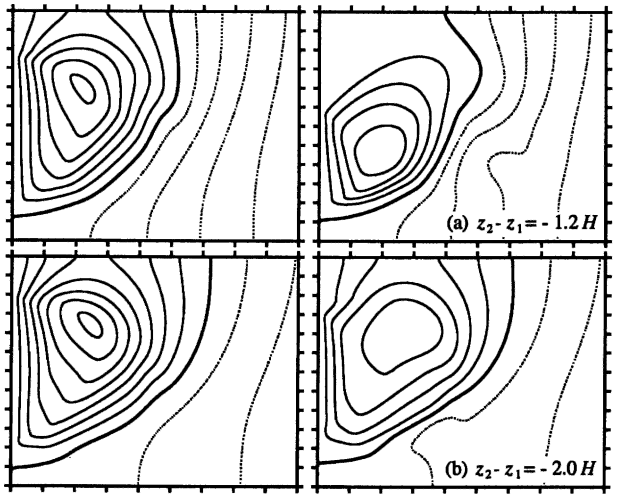

FIG. 11. Zonal mean zonal velocity, defined relative to the main (cyclonic) vortex centroid at (left) $t = 0$ and (right) $t = 10$ days, for the case $-\kappa_2/\kappa_1 = 0.2$ and for vertical offsets (a) $z_2 - z_1 = -1.2H$ and (b) $z_2 - z_1 = -2.0H$. Contours are the same as in Fig. 8.

Our motivation for this study stems from the work of O'Neill and Pope (1988) who identified coherent anticyclonic circulations associated with the stationary Aleutian high and eastward-traveling PV anomalies, situated on the equatorward flank of the polar vortex. Although the origin of these anomalies can be considered naturally in the framework of a wave–mean flow decomposition, their subsequent development resembles more closely the evolution of coherent vortical

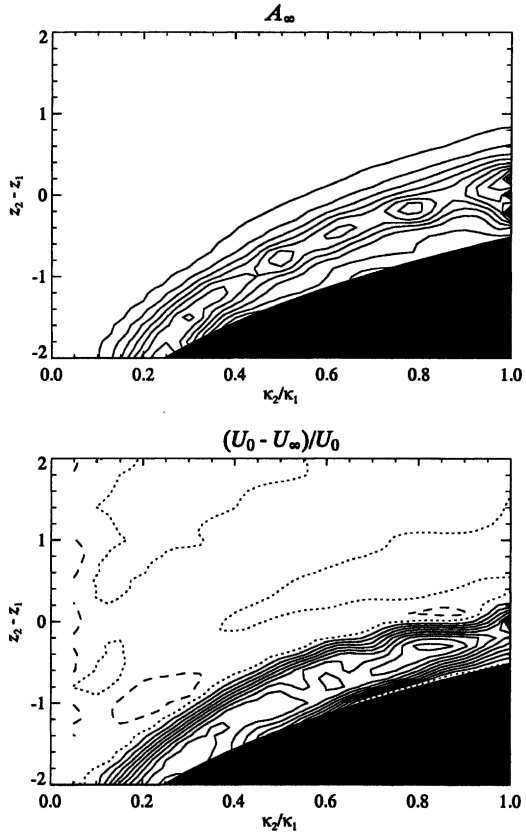

FIG. 12. Same as in Fig. 6, but for polar vortex centroid located at $z_1 = 4.5H$. Parameter values are constrained by the requirement that both vortices lie entirely within the vertical domain. Points on the boundary of the shaded region correspond to cases where the anticyclone exactly touches the ground.

structures, involving strongly local and nonlinear dynamics, for example during the merger of traveling and stationary anticyclones and the interaction of anticyclones with the polar vortex.

Observational evidence of equilibrium configurations consisting of a polar vortex and Aleutian high (or other anticyclonic circulations) has been documented in previous studies. The polar vortex and Aleutian high often coexist for relatively long periods without strong interaction. The cross sections of zonal wind shown in Figs. 5 and 9 of O'Neill et al. (1994) suggests a polar vortex that is tilted away from the weaker circulation of the Aleutian high with height, similar to the tilting discussed in section 3. Present meteorological analyses are now of sufficient resolution that accurate three-dimensional images of PV can be constructed throughout the stratosphere. It would be interesting to examine these datasets for further evidence of quasi-equilibrium states involving the polar vortex and Aleutian high, and to test the dependence of the morphology of equilibrium states predicted here on circulation strength and vertical offset.

The most dramatic instances of vortex–vortex interaction above occur for substantial circulation ratios, with $-\kappa_2/\kappa_1 \sim 0.6$–$0.8$. Certainly these values appear larger than anything that could be realistically attained in the polar stratosphere during winter radiative conditions. In the Southern Hemisphere late winter and spring, however, a strong stationary anticyclonic circulation, the Australian high, typically develops at the same time as the polar vortex is weakening through radiative processes. A striking example of the merger of this stationary anticyclone with an eastward-traveling anticyclone was discussed in Lahoz et al. (1996). Reconstructed maps of PV on the 1100-K isentropic surface suggest that the resulting anticyclonic circulation was indeed of comparable magnitude to the polar vortex. The examples of strong interaction shown here may therefore turn out to be more applicable to the dynamics of the Southern Hemisphere's final warming.

In general, and as to be expected, smaller circulation ratios resulted in less dramatic vortex–vortex interactions. However, an interesting result is that for very differently sized vortices, it is always the larger one that experiences the stronger deformations. That is, even a very weak anticyclonic circulation can induce large deformations to the polar vortex, and, if at the appropriate vertical offset, can result in shedding of vortex material and mean flow reduction similar to that observed in minor stratospheric warmings.

One important ingredient that might significantly enhance the potential for a weak anticyclone to induce strong polar vortex deformations is the presence of external forcing due, for example, to topography. O'Neill and Pope (1988) suggested that strong vortex interactions in the stratosphere relied on the presence of topographic forcing. While a full treatment of the effect of topography is clearly beyond the scope of the present work, an idea of its effect can be obtained by considering the unstable evolution of equilibria beginning farther within the margin of instability (closer together). This can be practically achieved by following the equilibrium finding procedure beyond the point where the deformation $\mathcal{M}$ exceeds $\mathcal{M}_c$. The weak external straining flow that brings the vortices together here is similar to the flow induced by topographic forcing. Under these conditions the interaction of a relatively weak anticyclone can be substantially enhanced. As an example, Fig. 13 shows the evolution for case with $-\kappa_2/\kappa_1 = 0.1$ and $z_2 - z_1 = 0$. While the anticyclone again remains relatively undeformed throughout the interaction, the polar vortex is this time violently deformed,

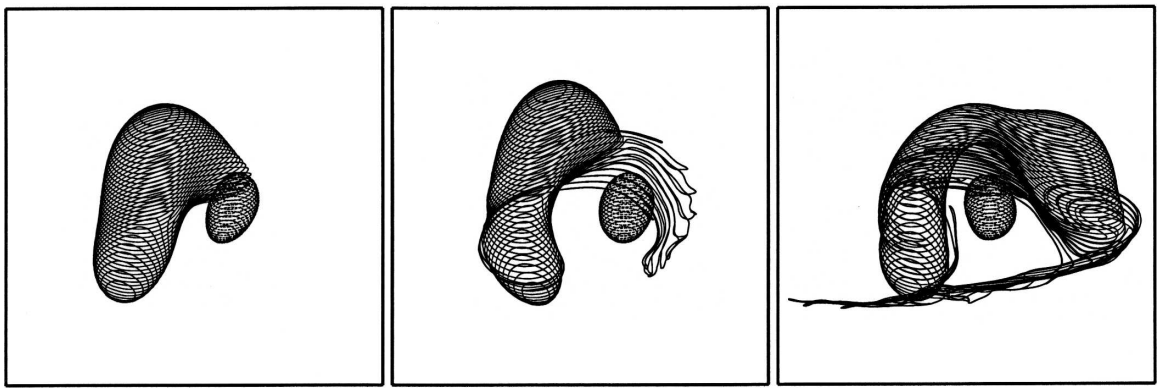

FIG. 13. Evolution for $-\kappa_2/\kappa_1 = 0.1$, $z_2 - z_1 = 0$ at $t = 0$, 8, and 16 days (left to right) in the presence of persistent external strain.

becoming strongly sheared in the vertical and eventually splitting in two. A similar shearing of the polar vortex occurred for other vertical offsets. The anticyclone in this case is half as strong as those presented in the weak interaction cases above—a mere 10% of the circulation of the polar vortex. The extent to which the instability of the two-vortex system manifests itself almost entirely through the destruction of the much larger polar vortex is remarkable.

Acknowledgments. Support for this research was provided by the U.K. Natural Environment Research Council under Grant NER/B/S/2002/00567.

REFERENCES

Christiansen, J. P., and N. J. Zabusky, 1973: Instability, coalescence and fission of finite-area vortex structures. *J. Fluid Mech.,* **61,** 219–243.

Dritschel, D. G., 1995: A general theory for two-dimensional vortex interactions. *J. Fluid Mech.,* **293,** 269–303.

——, and R. Saravanan, 1994: Three-dimensional quasi-geostrophic contour dynamics, with an application to stratospheric vortex dynamics. *Quart. J. Roy. Meteor. Soc.,* **120,** 1267–1297.

——, and M. H. P. Ambaum, 1997: A contour-advective semi-Lagrangian numerical algorithm for simulating fine-scale conservative dynamical fields. *Quart. J. Roy. Meteor. Soc.,* **123,** 1097–1130.

Esler, J. G., and R. K. Scott, 2005: Excitation of transient Rossby waves on the stratospheric polar vortex and the barotropic sudden warming. *J. Atmos. Sci.,* **62,** 3661–3682.

Harvey, V. L., and M. H. Hitchman, 1996: A climatology of the Aleutian high. *J. Atmos. Sci.,* **53,** 2088–2101.

Holton, J. R., 1976: A semi-spectral numerical model for wave, mean-flow interactions in the stratosphere: Application to sudden stratospheric warmings. *J. Atmos. Sci.,* **33,** 1639–1649.

Lahoz, W. A., and Coauthors, 1994: Three-dimensional evolution of water vapor distributions in the Northern Hemisphere stratosphere as observed by MLS. *J. Atmos. Sci.,* **51,** 2914–2930.

——, and Coauthors, 1996: Vortex dynamics and the evolution of water vapour in the stratosphere of the southern hemisphere. *Quart. J. Roy. Meteor. Soc.,* **122,** 423–450.

Legras, B., and D. G. Dritschel, 1993: Vortex stripping and the generation of high vorticity gradients in two-dimensional flows. *Appl. Sci. Res.,* **51,** 445–455.

Macaskill, C., W. E. P. Padden, and D. G. Dritschel, 2003: The CASL algorithm for quasi-geostrophic flow in a cylinder. *J. Comput. Phys.,* **188,** 232–251.

Matsuno, T., 1971: A dynamical model of the stratospheric sudden warming. *J. Atmos. Sci.,* **28,** 1479–1494.

McIntyre, M. E., and T. N. Palmer, 1983: Breaking planetary waves in the stratosphere. *Nature,* **305,** 593–600.

Newman, P. A., and E. R. Nash, 2005: The unusual Southern Hemisphere stratosphere winter of 2002. *J. Atmos. Sci.,* **62,** 614–628.

O'Neill, A., and V. D. Pope, 1988: Simulations of linear and nonlinear disturbances in the stratosphere. *Quart. J. Roy. Meteor. Soc.,* **114,** 1063–1110.

——, W. L. Grose, V. D. Pope, H. Maclean, and R. Swinbank, 1994: Evolution of the stratosphere during northern winter 1991/92 as diagnosed from U.K. Meteorological Office analyses. *J. Atmos. Sci.,* **51,** 2800–2817.

Pedlosky, J., 1987: *Geophysical Fluid Dynamics.* 2d ed. Springer, 710 pp.

Reinaud, J. N., and D. G. Dritschel, 2002: The merger of vertically offset quasi-geostrophic vortices. *J. Fluid Mech.,* **469,** 287–315.

Rosier, S. M., and B. N. Lawrence, 1999: The January 1992 stratospheric sudden warming: A role for tropical inertial instability? *Quart. J. Roy. Meteor. Soc.,* **125A,** 2575–2596.

Scott, R. K., and D. G. Dritschel, 2005: Quasi-geostrophic vortices in compressible atmospheres. *J. Fluid Mech.,* **530,** 305–325.